



HAL
open science

Pseudo-Curvature of Fractal Curves for Geometric Control of Roughness

Mohamad Janbein, Christian Gentil, Céline Roudet, Clément Poull

► **To cite this version:**

Mohamad Janbein, Christian Gentil, Céline Roudet, Clément Poull. Pseudo-Curvature of Fractal Curves for Geometric Control of Roughness. 19th International Conference on Computer Graphics Theory and Applications, Feb 2024, Rome, Italy. pp.177-188. hal-04474390

HAL Id: hal-04474390

<https://hal.science/hal-04474390v1>

Submitted on 26 Feb 2024

HAL is a multi-disciplinary open access archive for the deposit and dissemination of scientific research documents, whether they are published or not. The documents may come from teaching and research institutions in France or abroad, or from public or private research centers.

L'archive ouverte pluridisciplinaire **HAL**, est destinée au dépôt et à la diffusion de documents scientifiques de niveau recherche, publiés ou non, émanant des établissements d'enseignement et de recherche français ou étrangers, des laboratoires publics ou privés.

Pseudo-Curvature of Fractal Curves for Geometric Control of Roughness

Mohamad Janbein¹^a, Christian Gentil¹^b, Céline Roudet¹^c and Clement Poull¹^d

¹Laboratoire d'Informatique de Bourgogne (LIB), Université de Bourgogne, 9 Av. Alain Savary, 21000 Dijon, France
{mohamad.janbein, cgentil, celine.roudet, clement.poull}@u-bourgogne.fr

Keywords: curve, fractal geometry, Iterated Function System (IFS), nowhere differentiability, tangent, curvature.

Abstract: Fractal geometry is a valuable formalism for synthesizing and analyzing irregular curves to simulate non-smooth geometry or roughness. Understanding and controlling these geometries remains challenging because of the complexity of their shapes. This study focuses on the curvature of fractal curves defined from an Iterated Function System (a set of contractive operators). We introduce the *Differential Characteristic Function (DCF)*, a new tool for characterizing and analyzing their differential behavior. We associate a family of *DCF* to the fixed point of each operator. For each dyadic point of the curve, there exist left and right families of *DCF* inducing left and right ranges of curvatures: the *pseudo-curvatures*. A set of illustrations shows the influence of these pseudo-curvatures on the geometry of fractal curves. We propose a first approach for applying our results to roughness generation and control.

1 INTRODUCTION


Rough curves and surfaces have gained prominence in fields like quality control, computer-aided design, and computer graphics. They are utilized for diverse applications such as generating coherent terrains (Fournier et al., 1982; Warszawski et al., 2019), creating textures (Wang et al., 2021), or simulating their effects to replicate the light-matter interactions (Stam, 2001; Walter et al., 2007; Chermain et al., 2021) without adding geometric complexity.


There are different ways to produce roughness. In mathematics, roughness denotes irregularity in non-differentiable context. Quantifying such irregularity is established using mathematical constructs, like the Lipschitz coefficient and the Hölder coefficient in its various forms, pointwise, local, or global. Rough curves were first introduced by Bolzano (Bolzano, 1851; Thim, 2003), Weierstrass (Hardy, 1916) and Takagi (Allaart and Kawamura, 2012; Allaart and Kawamura, 2010). They follow an iterative construction, creating new details with decreasing amplitude related to the increasing frequency. This construction process results in a self-similar property related to fractal geometry (Mandelbrot, 1977), and fractal dimensions (Nayak et al., 2019). Another approach


to producing rough phenomena is to use statistical models. For example, the pioneer Perlin noise (Perlin, 1985) can produce rough-looking constructs with a high enough octave. However, many of these procedural noise models lack global control.


Designing and controlling the geometry of rough curves and surfaces is challenging. This paper aims to enrich the understanding of differential properties of fractal curves by studying curvature to provide tools for later designing and controlling rough curves and surfaces. Roughness is characterized by irregularities (differential behavior), often associated with self-similarity. Consequently, fractals offer an appropriate framework for studying phenomena related to roughness and irregularity. Deterministic is also essential for accurate controls and continuous dependency between parameters and resulting geometry. Consequently, we focus on fractal deterministic curves.

We review some related work in section 2. We focus on deterministic fractal curves defined by Iterated Function Systems (IFS) (Hutchinson, 1981) and projected IFS, as explained in section 3. Section 4 introduces the *differential characteristic function*, a new tool to analyze the differential behavior of fractal curves. Section 5 shows how the *differential characteristic functions* can be used to obtain known results about the tangent of a fractal curve. In section 6, we analyze the curvature at each fixed point from its associated family of *differential characteristic functions*, and we define the pseudo curvature of a fractal

^a <https://orcid.org/0000-0003-3271-0712>

^b <https://orcid.org/0000-0002-0343-3456>

^c <https://orcid.org/0000-0002-0704-081X>

^d <https://orcid.org/0000-0002-4402-2928>

curve. Finally section 7 discusses applying our results to roughness design and generation.

2 RELATED WORK

The automatic generation (for our purpose, geometries) implies having specifications, generally expressed in terms of expected properties or characteristic values. Of course, these specifications have to depend on the generator parameters. The nature of this dependency and its accessibility are central to having an intuitive control or facilitating the specification description.

Numerous studies deal with this question using spectral analysis to generate noises (fractal-based, colored noises, convolution noise) (Perlin, 1985; Cook and DeRose, 2005; Lagae et al., 2009; Gilet et al., 2014; Pavie, 2016; Cavalier et al., 2019; Hu and Tonder, 1992; Wang et al., 2021; Pérez-Ràfols and Almqvist, 2019). However, most need spectral control, which is only apparent with minimum knowledge. Other studies focus on the differential properties of random rough curves. In tribology, the contact area between two rough surfaces is analyzed from the curvature. Nowicki (Nowicki, 1985) lists and discusses numerous parameters for evaluating, analyzing, and modeling surface roughness. Some were concerned about differential properties like peak shapes, slope means, number of inflection points, and RMS of the profile slope, radius of asperity, and curvature radius. However, he only provides standard definitions for smooth curves without considering the numerical trouble caused by the irregularity of rough curves. Moalic et al. (Moalic et al., 1987) outline errors arising in the computation of slopes and curvatures statistical characteristics (mean, variance) for actual sampled surface. The tested methods by order of decreasing error are the finite difference methods (Whitehouse, 1982), the autospectrum approach, and the Fourier transform computation. However, all these methods evaluate the characteristics on average. Bigerelle et al. (Bigerelle et al., 2013) propose a method to calculate the curvature at any point of a random rough curve by considering the statistical self-similarity (fractal) property.

To eliminate the uncertainty of the randomness, some authors focus on deterministic curves. Daoudi et al. (Daoudi et al., 1998) construct nowhere differentiable continuous functions from prescribed local Hölder regularity at each point. However, the Hölder irregularity is a complex notion. Bensoudane and Podkorytov (Bensoudane et al., 2009; Podkorytov, 2013) focus on curves built with IFS and show

that it is possible to define left and right tangents even if the curve is nowhere differentiable. In some configurations, tangents are not defined, but the differential behavior is described by defining pseudo-tangents. These studies have shown accuracy brought by deterministic models. Pseudo-tangents are an interesting geometric tool for controlling roughness, but they are insufficient to manage the complexity of such curves. A second-order differential characteristic is expected.

3 BACKGROUND

An Iterated Function System (IFS) is a finite set of contractive operators $\{T_i\}_{i=0}^{I-1}$ that act on a complete metric space (\mathbb{X}, d) . For a given IFS, there exists a unique non-empty compact set A of (\mathbb{X}, d) satisfying the self-similarity property: $A = \bigcup_{i=0}^{I-1} T_i(A)$. Note that each operator T_i maps A onto a part of itself. A is called the attractor of the IFS. We compute it using the Hutchinson operator \mathbb{T} , defined by $\mathbb{T}(K) = \bigcup_{i=0}^{I-1} T_i(K)$, with $K \in H(\mathbb{X})$, the set of all non-empty compact subsets of \mathbb{X} . The attractor A can be obtained as the limit of an iterative process, given by $A = \lim_{i \rightarrow +\infty} \mathbb{T}^i(A)$.

Zair and Tosan (Zair and Tosan, 1996) and Schaefer (Schaefer et al., 2005) introduced the projected IFS model to create free-form fractal shapes that can be deformed by changing the positions of a set of N control points $P = \{P_0, \dots, P_{N-1}\}$. The attractor is defined in the barycentric space $BI^N = \left\{ \alpha \in \mathbb{R}^N \mid \sum_{j=0}^{N-1} \alpha_j = 1, \alpha = (\alpha_0, \dots, \alpha_{N-1})^T \right\}$ (Figure 1 left). Each point of $A \subset BI^N$ is interpreted as a set of weights w.r.t. the control points. The attractor is then projected onto the modeling space according to a set of control points P : $PA = \left\{ p \in \mathbb{X}, p = \sum_{j=0}^{N-1} \alpha_j P_j : \alpha \in A \right\}$ (see Figure 1 right).

This construction is similar to Bézier curves definition, where the Bernstein polynomial functions are defined in BI^N and then projected according to the set of control points: $C(t) = \sum_{j=0}^{N-1} B_j(t) P_j$. Note that Bézier (resp. NURBS) curves can be modeled using projected IFS (Zair and Tosan, 1996) (resp. C-IFS (Morlet et al., 2019)).

For the rest of the paper, all operators are contractive affine operators acting on BI^N . We consider the barycentric space BI^N as an hyperplane of the affine space \mathbb{R}^N , with the coordinate system of origin $O = (0, \dots, 0)$ and basis vectors $(\mathbf{e}_0, \dots, \mathbf{e}_{N-1})$ where the j^{th} component of the N -dimensional vector $(\mathbf{e}_i)_j = \delta_{ij}$, where δ_{ij} designates the Kronecker delta. The associated vector space of BI^N is the set of vec-

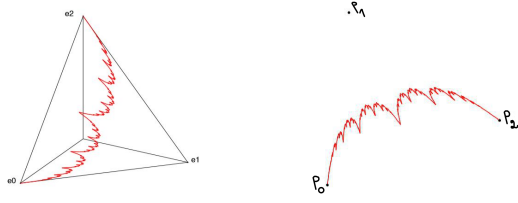


Figure 1: Left: Takagi attractor A built in the barycentric space BI^3 , where $\{\mathbf{e}_0, \mathbf{e}_1, \mathbf{e}_2\}$ are the canonical basis vectors. Right: projection of the attractor A of the left figure according to the set of control points $\{P_0, P_1, P_2\}$.

tors $\mathbf{BI}^N = \{\mathbf{v} \in \mathbb{R}^N \mid \sum_{j=0}^{N-1} \mathbf{v}_j = 0\}$. Consider an IFS $\{\mathbf{T}_i\}_{i=0}^{I-1}$, for each operator $\mathbf{T}_i : BI^N \rightarrow BI^N$, there exists a linear operator $\mathbf{T}_i : \mathbf{BI}^N \rightarrow \mathbf{BI}^N$ such that:

$$\mathbf{T}_i(x + \mathbf{v}) = \mathbf{T}_i(x) + \mathbf{T}_i(\mathbf{v}) \quad (1)$$

for any $x \in BI^N$ and any $\mathbf{v} \in \mathbf{BI}^N$. Each operator \mathbf{T}_i must be internal (a point of BI^N is mapped onto BI^N). As a consequence, their matrix form, expressed in the coordinate system $(O, \mathbf{e}_0, \dots, \mathbf{e}_{N-1})$, are $N \times N$ matrices with column's sum equals 1 (\mathbf{T}_i have the same matrix form as \mathbf{T}_i). Because of the constraint on the sum of each column, such matrices have 1 as eigenvalue. To be contractive, the remaining eigenvalues must have their modulus lesser than 1. For an operator \mathbf{T}_i , we adopt the following notation for its eigenvalues and eigenvectors: $(\lambda_i^0 = 1, \lambda_i^1, \dots, \lambda_i^{N-1})$ and $(\mathbf{v}_i^0, \mathbf{v}_i^1, \dots, \mathbf{v}_i^{N-1})$, respectively, where eigenvalues are arranged in decreasing modulus (upper index). The first eigenvector \mathbf{v}_i^0 (not in bold), associated to $\lambda_i^0 = 1$, corresponds to the fixed point, denoted by c_i . The sum of its components equals 1, meaning it is a point of BI^N . The other eigenvectors have the sum of their coordinates equal to zero, indicating that these eigenvectors are vectors. For example, we can consider the matrices of de Casteljaou, which are used in the calculation of Bézier curves:

$$\mathbf{T}_0 = \begin{pmatrix} 1 & 1/2 & 1/4 \\ 0 & 1/2 & 1/2 \\ 0 & 0 & 1/4 \end{pmatrix}, \quad \mathbf{T}_1 = \begin{pmatrix} 1/4 & 0 & 0 \\ 1/2 & 1/2 & 0 \\ 1/4 & 1/2 & 1 \end{pmatrix}$$

The attractor of the associated IFS is the Bernstein polynomial function of degree 2 lying in BI^3 .

With projected IFS, controlling the topology of such objects is challenging. An extension, named Boundary Controlled Iterated Function System (BC-IFS) (Sokolov et al., 2015; Gentil et al., 2021), provides a control of the attractor topology with incidence and adjacency constraints. Ensuring the $C^{(0)}$ continuity for curves is equivalent to applying the well-known constraints for Fractal Interpolation Functions (FIF) (Barnsley, 2014). We consider an IFS composed of two operators \mathbf{T}_0 and \mathbf{T}_1 that builds an attractor in BI^3 (as in Figure 2). The attractor is then

projected onto the modeling space using three control points $\{P_0, P_1, P_2\}$ defined in \mathbb{R}^2 . The operator \mathbf{T}_0 maps all the curve to the red part of the curve, and \mathbf{T}_1 maps it into the green part, so to guarantee that the two parts are connected, we impose the adjacency constraint for $C^{(0)}$: $\mathbf{T}_0 c_1 = \mathbf{T}_1 c_0$, where the fixed points c_0 and c_1 are the left and right endpoints of the curve respectively (see Figure 2).

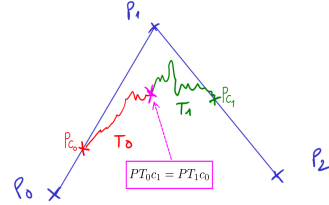


Figure 2: Adjacency constraint for $C^{(0)}$ continuity: $\mathbf{T}_0 c_1 = \mathbf{T}_1 c_0$ is imposed for the IFS composed of \mathbf{T}_0 and \mathbf{T}_1 to guarantee the connectivity of the fractal curve at the joining point, the curve is then projected into the modeling space with control points $\{P_0, P_1, P_2\}$.

We define dyadic points, on which we compute the pseudo-curvature as following: $p \in A$ is a dyadic point if there exists a finite sequence of indices $\sigma_0, \sigma_1, \dots, \sigma_l$ (where $\sigma_i \in \{0, \dots, I-1\}$ and $\sigma_{l-1} \neq \sigma_l$) s.t. $p = \mathbf{T}_{\sigma_0} \mathbf{T}_{\sigma_1} \dots \mathbf{T}_{\sigma_{l-1}} c_{\sigma_l}$.

4 CHARACTERIZATION OF ITERATIVE BEHAVIORS

The main idea of this paper is to consider an attractor as a set of sequences. We know that each \mathbf{T}_i has a fixed point c_i belonging to the attractor. By applying \mathbf{T}_i iteratively on the fixed point c_k of another operator \mathbf{T}_k , we define a sequence of points converging to c_i , each element of the sequence belonging to the attractor.

This section introduces the *differential characteristic function (DCF)* to formalize and simplify these sequences' behavior.

4.1 Elementary Iterative Behavior of One Operator

Consider an internal contractive operator T (of an IFS defining a curve) acting on BI^3 , $(\lambda^0 = 1, \lambda^1, \lambda^2)$ its eigenvalues, $(\mathbf{v}^0 = c, \mathbf{v}^1, \mathbf{v}^2)$ its eigenvectors and q_0 a point of BI^3 .

We define the sequence $\{q_n\}_{n \in \mathbb{N}}$ by: $q_n = T^n q_0$. Each term of this resulting sequence can be expressed

in the coordinate system $\{c, \mathbf{v}^1, \mathbf{v}^2\}$:

$$q_0 = c + x_1 \mathbf{v}^1 + x_2 \mathbf{v}^2, \text{ where } x_1, x_2 \in \mathbb{R} \quad (2)$$

$$T^n q_0 = T^n c + T^n(x_1 \mathbf{v}^1 + x_2 \mathbf{v}^2) \quad (3)$$

$$T^n q_0 = c + x_1 (\lambda^1)^n \mathbf{v}^1 + x_2 (\lambda^2)^n \mathbf{v}^2 \quad (4)$$

To gain insight into the differential properties of the curve, we need to analyze the different behaviors of the sequence $\{q_n\}_{n \in \mathbb{N}}$ w.r.t. the eigensystem of T . To see clearly these behaviors, we project the sequence of points $T^n q_0$ onto the modeling space in a way to have an orthogonal system $\{Pc, P\mathbf{v}^1, P\mathbf{v}^2\}$ such that $\|P\mathbf{v}^1\| = \|P\mathbf{v}^2\|$ and then $\|P\lambda^1 \mathbf{v}^1\|$ and $\|P\lambda^2 \mathbf{v}^2\|$ reflect the value of the eigenvalues (as shown in the figures below). The different cases are defined from the eigenvalues:

- Case 1: if $|\lambda^1| > |\lambda^2| > 0$, the contraction in the direction of \mathbf{v}^2 is greater than that in the direction of \mathbf{v}^1 , the sequence converges to the point Pc tangentially to the eigenvector \mathbf{v}^1 . Figure 3 left illustrates the different configurations according to the location of the starting point in the four quadrants defined from the eigenvectors.
- Case 2: if $|\lambda^1| > |\lambda^2|$, $\lambda^1 < 0$ and $\lambda^2 < 0$, the components $x_1 (\lambda^1)^n$ and $x_2 (\lambda^2)^n$ of q_n alternates between positive and negative values as a function of n , and therefore the sequence of points passes alternately from the starting quadrant to the opposite one (Figure 3 right).

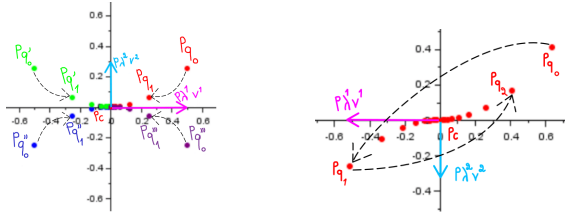


Figure 3: Left: Applying T (with eigenvalues $\lambda^1 > \lambda^2$) on four different starting points ($Pq_0, Pq'_0, Pq''_0, Pq'''_0$). Each sequence converges to Pc tangentially to $P\mathbf{v}^1$. Right: $\lambda^1 < 0$ and $\lambda^2 < 0$: the sequence of points $\{PT^n q_0\}_{n \in \mathbb{N}}$ alternates between the starting quadrant to the opposite one until converging towards the point Pc .

- Case 3: if $|\lambda^1| > |\lambda^2| > 0$ and $\lambda^1 < 0$, the component $x_1 (\lambda^1)^n$ of q_n alternates between positive and negative values as a function of n , and therefore the sequence of points passes alternately from one of the half-planes delimited by the line $c + t\mathbf{v}^2$ to the other half-plane (Figure 4 left).
- Case 4: if $\lambda^1 > |\lambda^2|$ and $\lambda^2 < 0$, the component $x_2 (\lambda^2)^n$ of q_n alternates between positive and negative values as a function of n , and therefore the sequence of points passes alternately from one of

the half-planes delimited by the line $c + t\mathbf{v}^1$ to the other half-plane. But the sequence already converges to c tangentially to \mathbf{v}^1 (Figure 4 right).

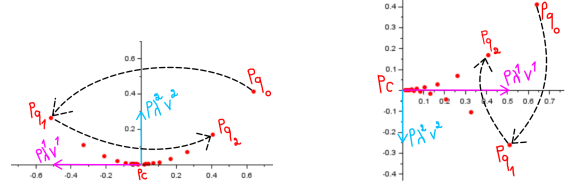


Figure 4: In both figures, the sequences of points $\{PT^n q_0\}_{n \in \mathbb{N}}$ converge to the point Pc . They alternate between the positive and negative half-planes delimited by the second eigenvector $P\lambda^2 \mathbf{v}^2$ (for the left figure, where $\lambda^1 < 0$) or by the first one $P\lambda^1 \mathbf{v}^1$ (for the right figure, where $\lambda^2 < 0$).

- Case 5: $\lambda^1 = \lambda^2 > 0$, the contractions in the directions of \mathbf{v}^1 and \mathbf{v}^2 are equal, and the sequence of points converges on a straight line to the point Pc .
- Case 6: if $\lambda^1 = \bar{\lambda}^2$ are complex eigenvalues, the operator is characterized by a rotation, and the sequence of points converges on a spiral to the point Pc .

4.2 The Differential Characteristic Function

In order to analyze the differential properties at the fixed point c of a contractive operator T , we aim to find an analytical function that interpolates the points of the sequence obtained by applying T on a starting point q_0 . This expression will allow a formal characterization of the differential behavior at the limit point of the sequence.

We first focus on the simplest case with T acting on BI^3 and where both λ^1 and λ^2 are positive (i.e. $1 > \lambda^1 > \lambda^2 > 0$). We will present the other configurations later.

Definition: Consider an operator T acting on BI^3 with eigenvalues ($\lambda^0 = 1 > \lambda^1 > \lambda^2 > 0$) and associated eigenvectors ($\mathbf{v}^0 = c, \mathbf{v}^1, \mathbf{v}^2$). We suppose \mathbf{v}^1 and \mathbf{v}^2 independent. Let q be a point of $BI^3 \setminus \{c + t\mathbf{v}^2\}_{t \in \mathbb{R}}$ (i.e. q does not belong to the line passing through c in the direction of \mathbf{v}^2), and consider its expression in the coordinates system $(c, \mathbf{v}^1, \mathbf{v}^2)$: $q = c + x_1 \mathbf{v}^1 + x_2 \mathbf{v}^2$. We suppose that \mathbf{v}^1 and \mathbf{v}^2 are chosen such that $x_1 > 0$ and $x_2 > 0$. The *differential characteristic function (DCF)* is defined by:

$$D_{T,q}(t) = c + t\mathbf{v}^1 + \beta t^\alpha \mathbf{v}^2, \quad t \in \mathbb{R}^+ \quad (5)$$

where $\beta = \frac{x_2}{(x_1)^\alpha}$ and $\alpha = \frac{\log(\lambda^2)}{\log(\lambda^1)}$.

Property: D_{T,q_0} interpolates the points of the sequence $\{q_n\}_{n \in \mathbb{N}} = \{T^n q_0\}_{n \in \mathbb{N}}$ (see Figure 5 left).

Proof. $q_0 = c + x_1 \mathbf{v}^1 + x_2 \mathbf{v}^2$, where $x_1, x_2 \in \mathbb{R}^{+*}$

$$\begin{aligned} q_n = T^n q_0 &= c + x_1 (\lambda^1)^n \mathbf{v}^1 + x_2 (\lambda^2)^n \mathbf{v}^2 \\ &= c + X_1 \mathbf{v}^1 + X_2 \mathbf{v}^2 \end{aligned}$$

We have to prove that q_n have their coordinates (X_1, X_2) in the form $(t, \beta t^\alpha)$. Set $t = X_1 = x_1 (\lambda^1)^n$ then: $\beta t^\alpha = \beta (x_1 (\lambda^1)^n)^\alpha = \frac{x_2}{(x_1)^\alpha} (x_1)^\alpha ((\lambda^1)^n)^\alpha$. Because $\alpha = \frac{\log(\lambda^2)}{\log(\lambda^1)}$, $\lambda^2 = (\lambda^1)^\alpha$, $x_2 (\lambda^2)^n = \beta t^\alpha$ and $X_2 = \beta t^\alpha$. \square

Property: The graph of $D_{T,q}(t)$, denoted by $Graph(D_{T,q})$, is invariant under T .

Proof. Consider a DCF $D_{T,q}(t) = c + t\mathbf{v}^1 + \beta t^\alpha \mathbf{v}^2$. Let m be a point of $Graph(D_{T,q})$, $m = c + t_m \mathbf{v}^1 + \beta t_m^\alpha \mathbf{v}^2$. Then $Tm = c + \lambda^1 t_m \mathbf{v}^1 + \lambda^2 \beta t_m^\alpha \mathbf{v}^2$ and as $\lambda^2 = (\lambda^1)^\alpha$, $Tm = c + \lambda^1 t_m \mathbf{v}^1 + \beta (\lambda^1 t_m)^\alpha \mathbf{v}^2 \in Graph(D_{T,q})$ \square

Remark: If $s \notin Graph(D_{T,q})$, then $\beta_s \neq \beta$, and $D_{T,s}$ is different from $D_{T,q}$ (see Figure 5 right).

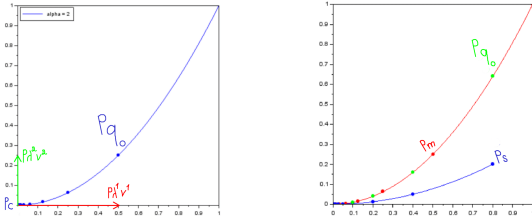


Figure 5: Various DCFs $D_{T,q}(t) = c + t\mathbf{v}^1 + \beta t^\alpha \mathbf{v}^2$ with different starting points (q_0, m or s). In the right figure, D_{T,q_0} (in red) interpolates both green and red sequences of points $\{PT^n q_0\}_{n \in \mathbb{N}}$ and $\{PT^n m\}_{n \in \mathbb{N}}$ (with $m \in Graph(D_{T,q_0})$). In blue, $D_{T,s}$ ($s \notin Graph(D_{T,q_0})$) interpolates the blue sequence of points.

In the definition of the DCF, we previously imposed conditions on λ^1 and λ^2 . We discuss here the general configuration. For the specific cases where x_1 or x_2 are null, D_{T,q_0} is defined as follows: if $x_1 = 0$ then $D_{T,q_0}(t) = c + t\mathbf{v}^2$ and if $x_2 = 0$ then $D_{T,q_0}(t) = c + t\mathbf{v}^1$. If both x_1 and x_2 are null D_{T,q_0} is not defined ($q_0 = c$ the fixed point of T). If λ^1 and/or λ^2 are strictly negative, we define a double DCF, one interpolating the sequence of points $\{PT^n q_0\}_{n \in \mathbb{N}}$ with even values of n , and one for odd values:

- Case 1: λ^1 and λ^2 are strictly negative (see Fig 6):
 - $D_{T,q_0}^1(t) = c + t\mathbf{v}^1 + \beta t^\alpha \mathbf{v}^2$ for even values of n .
 - $D_{T,q_0}^2(t) = c - t\mathbf{v}^1 - \beta t^\alpha \mathbf{v}^2$ for odd values of n .
- Case 2: λ^1 strictly negative (see Fig 7 left):
 - $D_{T,q_0}^1(t) = c + t\mathbf{v}^1 + \beta t^\alpha \mathbf{v}^2$ for even values of n .
 - $D_{T,q_0}^2(t) = c - t\mathbf{v}^1 + \beta t^\alpha \mathbf{v}^2$ for odd values of n .

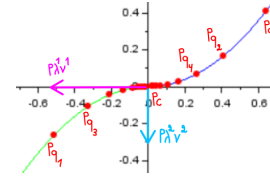


Figure 6: $\lambda^1 < 0$ and $\lambda^2 < 0 \Rightarrow$ double DCF, the first one in blue interpolating the points of the sequence $\{PT^n q_0\}_{n \in \mathbb{N}}$ for even indices, and the second one in green for odd indices.

- Case 3: λ^2 strictly negative (see Fig 7 right):
 - $D_{T,q_0}^1(t) = c + t\mathbf{v}^1 + \beta t^\alpha \mathbf{v}^2$ for even values of n .
 - $D_{T,q_0}^2(t) = c + t\mathbf{v}^1 - \beta t^\alpha \mathbf{v}^2$ for odd values of n .

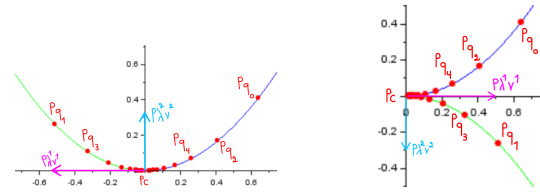


Figure 7: For both figures, two DCFs are shown with different colours. The blue one interpolates the points of the sequence $\{PT^n q_0\}_{n \in \mathbb{N}}$ with even indices, the green one for odd indices. $\lambda^1 < 0$ for the left figure and $\lambda^2 < 0$ for the right one.

- Case 4: λ^1 strictly negative and $|\lambda^1| = \lambda^2 > 0$:
 - $D_{T,q_0}^1(t) = c + t\mathbf{v}^1 + \beta t^\alpha \mathbf{v}^2$ for even values of n .
 - $D_{T,q_0}^2(t) = c - t\mathbf{v}^1 + \beta t^\alpha \mathbf{v}^2$ for odd values of n .

Now, consider a fractal curve defined in a barycentric space BI^N , from a set of I operators $\{T_i\}_{i=0}^{I-1}$. For a given operator T_i and from each point q_0 of the curve, we can define a sequence of points $\{q_n\}_{n \in \mathbb{N}}$ belonging to the curve and consequently a simple or double DCF. Figure 8 shows a fractal curve in BI^4 defined from an IFS composed of two operators T_0 and T_1 , and projected into the modeling space using four control points. This curve has many points having different values of β . Applying T_0 iteratively to these points results in many sequences of points converging to the left endpoint c_0 , such as the two sequences displayed in blue and black in the figure with their corresponding DCFs. Let us denote the set of all DCFs representing all sequences converging to c_i by:

$$FDCF(i) = \{D_{T_i, q_0}, q_0 \in A\} \quad (6)$$

In the following section, we will analyze $FDCF(i)$ to characterize the differential behavior in the neighborhood of c_i . Then, we will propagate these results to dyadic points thanks to the self-similarity property.

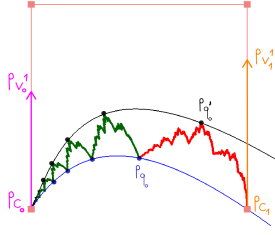


Figure 8: In blue and black, the two different sequences obtained by applying T_0 iteratively to P_{q_0} and $P_{q'_0}$ are converging to the limit point P_{c_0} .

5 PSEUDO-TANGENT PROPERTIES OF FRACTAL CURVES USING DCF

In this section, we show how we obtain known results given by Bensoudane et al. (Bensoudane, 2009).

Let us consider a fractal curve defined in the barycentric space BI^N , from a set of I operators $\{T_i\}_{i=0}^{I-1}$. The differential behavior of a sequence of points can be directly determined from the derivative of D_{T_i, q_0} . According to the different configurations:

- $D'_{T_i, q_0}(t) = \pm \mathbf{v}_i^1 \pm \beta \alpha^{\alpha-1} \mathbf{v}_i^2$, when $x_1 \neq 0$ and $x_2 \neq 0$,
- $D'_{T_i, q_0}(t) = \pm \mathbf{v}_i^1$, when $x_2 = 0$,
- or $D'_{T_i, q_0}(t) = \pm \mathbf{v}_i^2$, when $x_1 = 0$.

The tangent at $t = 0$ is:

- If $\alpha > 1$, $D'_{T_i, q_0}(0) = \pm \mathbf{v}_i^1$ (if $x_1 \neq 0$) or $D'_{T_i, q_0}(0) = \pm \mathbf{v}_i^2$ (if $x_1 = 0$).

The derivative depends only on which quadrant q_0 belongs.

- If $\alpha = 1$, $D'_{T_i, q_0}(0) = \pm \mathbf{v}_i^1 \pm \beta \mathbf{v}_i^2$.

The derivative depends on the position of q_0 .

This means that if all curve points satisfy the same conditions in terms of x_1 and x_2 , all iterative sequences will converge to the fixed point with the same tangent.

Note that the tangent lies in the barycentric space. The tangent of the projected curve according to the set of control points is $PD'_{T_i, q_0}(0)$ (the projection conserves the collinearity). To have a unique behavior for all DCF of a FDCF(i), we need to impose common constraints on all the points of the curve. These constraints are expressed in terms of $sign(x_1)$ and/or $sign(x_2)$. To present this analysis without ambiguity, we consider the tangent itself and the direction of the finite difference at t : $\Delta_h[C](t) = C(t+h) - C(t)$, where $C([0, 1]) = A$ denotes the parameterised fractal curve (with $C(0) = c_0$ and $C(1) = c_1$). In the following cases, we show different configurations with associated example curves. Each curve is generated by an

IFS composed of two operators in BI^3 and then is projected into \mathbb{R}^2 by a set of three control points (black squares). We focus on T_0 and we only display D_{T_0, c_1} (in green). For each figure, x_1 and x_2 represents the coordinates of c_1 in $(c_0, \mathbf{v}_0^1, \mathbf{v}_0^2)$. The constraints on x_1 and x_2 must be satisfied for all q belonging to the curve:

- Case 1: $\lambda_0^1 > 0$ and $\lambda_0^2 > 0$, $x_1 > 0$ and $x_2 > 0 \Rightarrow$ the tangent at P_{c_0} is Pv_0^1 (Figure 9 left).
- Case 2: $\lambda_0^1 < 0$ and $\lambda_0^2 < 0 \Rightarrow$ the tangent at P_{c_0} oscillates indefinitely between Pv_0^1 and $-Pv_0^1$ (Figure 9 right).

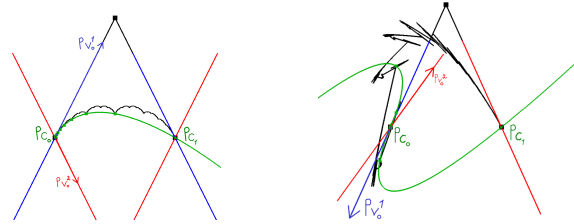


Figure 9: Left: the tangent at P_{c_0} is Pv_0^1 . Right: at P_{c_0} , $\Delta_h[C](0)$ oscillates indefinitely between Pv_0^1 and $-Pv_0^1$, while h tends to zero.

- Case 3: $\lambda_0^1 > 0$ and $\lambda_0^2 < 0$, $x_1 > 0 \Rightarrow$ the tangent at P_{c_0} is Pv_0^1 (Figure 10 left).
- Case 4: $\lambda_0^1 < 0$ and $\lambda_0^2 > 0$, $x_2 > 0 \Rightarrow$ the tangent at P_{c_0} oscillates indefinitely between Pv_0^1 and $-Pv_0^1$ (Figure 10 right).

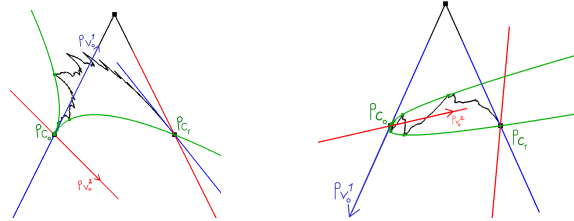


Figure 10: Left: the tangent at P_{c_0} is Pv_0^1 . Right: at P_{c_0} , $\Delta_h[f](0)$ oscillates indefinitely between Pv_0^1 and $-Pv_0^1$, while h tends to zero.

- Case 5: $|\lambda_0^1| = \lambda_0^2 > 0$, $x_1 > 0 \Rightarrow$ the tangent is not defined at P_{c_0} , it oscillates indefinitely between two extrema (Figure 11).

This analysis can be carried out on both ending points of the curve. Then, by the self-similarity property, each behavior is transported to the right and left sides of each dyadic point. All possible combinations can be obtained. In case where an eigenvalue is complex, it reflects a rotation component in the operator, introduces a spiral around the fixed points.

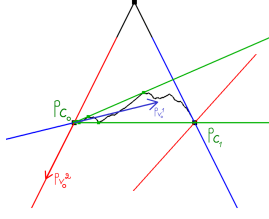


Figure 11: In c_0 , $\Delta_h[f](0)$ oscillates indefinitely between two extrema depending on the geometry of the curve, while h tends to zero.

6 PSEUDO-CURVATURE OF FRACTAL CURVES

In the previous section, we showed that even if fractal curves are generally nowhere differentiable, it is possible, with some conditions, to define right and left tangents. In this section, we focus on the curvature to assess the impact of the second derivative on the curve. The curvature presents the first advantage of being independent of the parametrization, which is not apparent to manage for fractal curves. Our idea is to study the curvature of a fractal through the second derivative of the *FDCF*.

6.1 Curvature Analysis of a DCF

First, we focus on the curvature at the left and right endpoints of the curve. For a given parametric curve $f(t)$, the curvature $\kappa(t)$ is:

$$\kappa(t) = \frac{\|f'(t) \times f''(t)\|}{\|f'(t)\|^3} \quad (7)$$

Consider an operator T (of an IFS defining a curve) acting on BI^3 , ($v^0 = c, v^1, v^2$) its eigenvectors and q_0 a point of BI^3 . For the simplicity of calculations, we project the sequence of points $\{T^n q_0\}_{n \in \mathbb{N}}$ onto the modeling space in a way to have an orthogonal system $\{Pc, Pv^1, Pv^2\}$ such that $\|Pv^1\| = \|Pv^2\|$ (the general case will be given later). From a given point q_0 belonging to the curve, we can determine the curvature of PD_{T,q_0} :

$$\kappa(t) = \frac{\|PD'_{T,q_0}(t) \times PD''_{T,q_0}(t)\|}{\|PD'_{T,q_0}(t)\|^3} \quad (8)$$

Note that we compute the curvature directly in the modeling space (i.e. from the projected curves) because the cross-product has no meaning in the barycentric space. We have:

$$PD'_{T,q_0}(t) = Pv^1 + \beta\alpha t^{\alpha-1} Pv^2 \quad (9)$$

$$PD''_{T,q_0}(t) = \beta\alpha(\alpha-1)t^{\alpha-2} Pv^2 \quad (10)$$

Pv^1 and Pv^2 are chosen orthonormal, then:

$$\kappa(t) = \frac{|\beta\alpha(\alpha-1)t^{\alpha-2}|}{(1 + (\beta\alpha t^{\alpha-1})^2)^{3/2}} \quad (11)$$

Using the tangent existence constraint: $0 < |\lambda_2| < \lambda_1 < 1$ we can deduce the domain of α :

$$1 < \frac{\log(|\lambda_2|)}{\log(\lambda_1)} = \alpha < +\infty \quad (12)$$

We can distinguish three different cases for the value $\kappa(t)$ at $t = 0$, depending on the value of α :

- Case 1: if $1 < \alpha < 2 \Rightarrow \lim_{t \rightarrow 0} \kappa(t) = +\infty$, Figure 12 left shows in blue the curve PD_{T,q_0} and Figure 12 right the corresponding curvature. When t tends to zero, the curvature tends to $+\infty$.

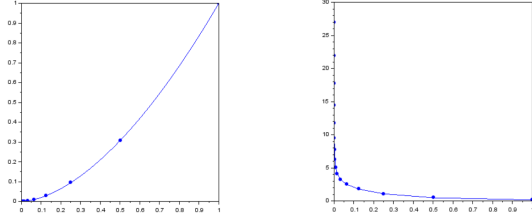


Figure 12: Left: the curve PD_{T,q_0} having $1 < \alpha < 2$. Right: the curvature values of the curve displayed on the left figure.

- Case 2: if $\alpha = 2$ ($\lambda_2 = \lambda_1^2$) $\Rightarrow \kappa(0) = |2\beta| \neq 0$. Figure 13 left shows in blue the curve PD_{T,q_0} and Figure 13 right the corresponding curvature. When t tends to zero, the curvature tends to a finite non-zero value depending on β . This case induces a correspondence between the second derivative PD''_{T,q_0} and the second eigenvector Pv^2 at the fixed point Pc ($PD''_{T,q_0}(0)$ collinear to Pv^2).
- Case 3: if $\alpha > 2$, as the curve in red (Figure 13 left) approaches the fixed point Pc , $\lim_{t \rightarrow 0} \kappa(t) = 0$ (Figure 13 right).

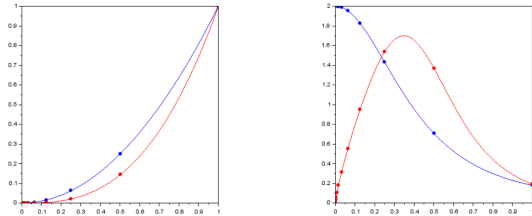


Figure 13: Left: in red, the curve PD_{T,q_0} where $\alpha > 2$. In blue, the curve PD_{T,q_0} where $\alpha = 2$. Right: the corresponding curvature values for the red and blue curves displayed on the left figure.

Thanks to D_{T,q_0} , we can characterize the differential behavior of the sequence $\{q_n\}_{n \in \mathbb{N}}$ at the fixed

point of an operator. In the first and third cases, the curvature is either zero or infinite and does not depend on the value of β . While in the case where $\alpha = 2$, the curvature is finite, non-zero and depends on the initial point q_0 (see Figure 14).

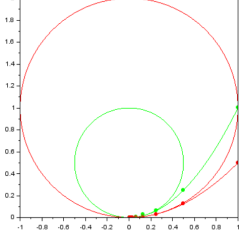


Figure 14: Two starting points (on the right) having distinct $\beta \Rightarrow$ two distinct *DCF*s (curves in red and green) having two different curvatures represented by their red and green osculating circles at the limit point.

6.2 Curvature of a *DCF* in BI^3 and BI^N

In the previous section, when we have considered an operator T acting on BI^3 , we have made the assumption that $\{Pc, P\mathbf{v}^1, P\mathbf{v}^2\}$ is an orthogonal system. Later, we adapt the previous results to the general case in BI^3 and after in BI^N , for an IFS $\{T_0, T_1\}$.

Let us consider $\{\mathbf{i}, \mathbf{j}\}$ the canonical orthonormal basis of \mathbb{R}^2 . We denote the decomposition of each projected eigenvector of an operator T_i by: $P\mathbf{v}_i^k = a_k \mathbf{i} + b_k \mathbf{j}$ for $k \in \{1, 2\}$.

Then for each $PD_{T_i, q}(t)$:

$$\kappa(t) = \frac{|(a_1 b_2 - b_1 a_2) \beta_i \alpha_i (\alpha_i - 1) t^{\alpha_i - 2}|}{|a_1^2 + b_1^2 + 2(a_1 a_2 + b_1 b_2) \beta_i \alpha_i t^{\alpha_i - 1} + (a_2^2 + b_2^2) (\beta_i \alpha_i t^{\alpha_i - 1})^2|^{\frac{3}{2}}} \quad (13)$$

From this formula and because $1 < \alpha_i = \frac{\log(|\lambda_i^z|)}{\log(|\lambda_i^1|)} < +\infty$, we have the same cases as the previous simple section:

- Case 1: $1 < \alpha_i < 2$: $\alpha_i - 2 < 0$ then $\lim_{t \rightarrow 0} \kappa(t) = +\infty$.
- Case 2: $\alpha_i = 2$ then $\kappa(0)$ is finite and non-zero.

$$\text{The curvature at } c_i : \kappa(0) = \frac{|2\beta_i(a_1 b_2 - b_1 a_2)|}{(a_1^2 + b_1^2)^{\frac{3}{2}}}$$

depends on β_i . This case induces a correspondence between the second derivative D''_{T_i, q_0} and the second eigenvector \mathbf{v}_i^2 at c_i ($D''_{T_i, q_0}(0)$ collinear to \mathbf{v}_i^2).

- Case 3: $\alpha_i > 2$: $\lim_{t \rightarrow 0} \kappa(t) = 0$.

In general, a *DCF* lies in an N -dimensional barycentric space BI^N . Operators T_i are represented by $N \times N$ matrices, with at most N eigenvalues and N eigenvectors. The eigenvalues have

the following condition: $\lambda_i^0 = 1 > \lambda_i^1 > |\lambda_i^2| > \dots > |\lambda_i^{N-1}| > 0$. Consider a starting point $q_0 = c_i + x_1 \mathbf{v}_i^1 + \dots + x_{N-1} \mathbf{v}_i^{N-1} \in A$ where $x_1, \dots, x_{N-1} \in \mathbb{R}$, the *DCF* which interpolates the obtained sequence of points $\{q_n\}_{n \in \mathbb{N}}$ (in BI^N) becomes:

$$D_{T_i, q_0} = c_i + t \mathbf{v}_i^1 + \beta_{i,2} t^{\alpha_{i,2}} \mathbf{v}_i^2 + \dots + \beta_{i,N-1} t^{\alpha_{i,N-1}} \mathbf{v}_i^{N-1} \quad (14)$$

where $\alpha_{i,z} = \frac{\log(|\lambda_i^z|)}{\log(|\lambda_i^1|)}$, and $\beta_{i,z} = \frac{x_z}{x_{z-1}}$ for $2 \leq z \leq N-1$, and its curvature is more complex, but when t tends to zero, most of the terms vanish, and we obtain the same cases as for BI^3 .

6.3 Pseudo-curvature and *FDCF*

As defined in section 5, we associate to each fixed point c_i a *FDCF*(i). This family is defined from all the points belonging to the curve and having different values of β . As we show in sections 6.1 and 6.2, we identify three identical cases, depending only on $\alpha_{i,2}$. For cases where $1 < \alpha_{i,2} < 2$ and $\alpha_{i,2} > 2$, the curvature doesn't depend on $\beta_{i,2}$, meaning all *DCF* of *FDCF*(i) have the same curvature which is infinite and 0 respectively. Then we state that the pseudo curvature of the fractal curve at c_i is the common curvature of *FDCF*(i).

For the remaining case, where $\alpha_{i,2} = 2$, the curvature is in the form:

$$\kappa_i(0) = \frac{|2\beta_{i,2} \times cst_1|}{cst_2}, \quad (15)$$

where cst_1 and cst_2 denote two real constants. If all points q_0 belonging to the fractal curve except the point c_i ($A \setminus \{c_i\}$) satisfy $x_1 > 0$ and $x_2 > 0$ (implying $\lambda_i^1 > 0$ and $\lambda_i^2 > 0$), the set $\{\beta_{i,2}, \text{ s.t. } q_0 \in A\}$ have a lower and an upper bound, $\beta_{i,inf}$ and $\beta_{i,sup}$ respectively. The curve is embedded in the area defined by all the graphs of *FDCF*(i) as the Figure 15 shows. *FDCF*(i) induces a range of curvatures bounded by $\kappa_{i,inf} = \frac{|2\beta_{i,inf} \times cst_1|}{cst_2}$ and $\kappa_{i,sup} = \frac{|2\beta_{i,sup} \times cst_1|}{cst_2}$. In this case, the behavior of the curve is too complex to be approximated by a unique circle. We define the pseudo curvature of the fractal curve at c_i by the interval $[\kappa_{i,inf}, \kappa_{i,sup}]$, implying a continuous set of osculating circles (see Figure 17).

We can observe different situations according to the signs of λ_i^1 and λ_i^2 . For example, in Figure 16, $1 > \lambda_i^1 > |\lambda_i^2| > 0$ and $\lambda_i^2 < 0$. As explained in section 3.2, considering the computation of the curvature at c_i , we have a double *DCF* for each sequence of points converging to c_i . This involves a range of curvature for both sides of c_i w.r.t. \mathbf{v}_i^1 , with the same value of κ_{sup} . As the curve passes through the line $c_i + t \mathbf{v}_i^1$, there exist points s.t. $x_2 = 0$ and defining a *DCF* with

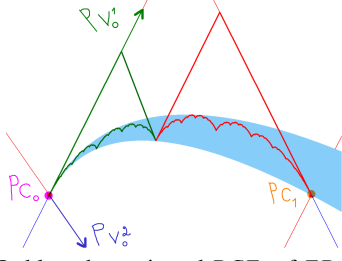


Figure 15: In blue, the projected DCF s of $FDCF(0)$ cover the fractal curve.

a null curvature. The pseudo-curvature is the range of curvature defined from $FDCF(i)$ as a set of curvatures ranging in $[0, \kappa_{i,sup}]$ for both sides of the line $c_i + tv_i^1$.

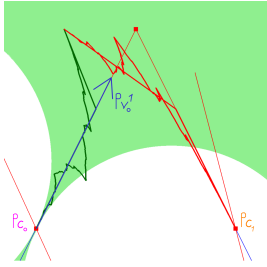


Figure 16: In green, we show the range of the right pseudo-curvature at the left endpoint c_0 , where $0 \leq \kappa \leq 0.659$ and $\lambda_0^2 = -(\lambda_0^1)^2 = -0.36$.

When $\lambda_i^1 < 0$ and $\lambda_i^2 > 0$, we can do the analysis symmetrically to the previous one. As the curve passes through the line $c_i + tv_i^2$, there exist points s.t. $x_1 = 0$ and defining a DCF with the value of curvature equals 0. For both sides of the line $c_i + tv_i^2$, as the point of the curve approaches the line, the curvature of the corresponding DCF tends to infinity. But it although exists $\kappa_{i,inf}$ as the curve is compact. The pseudo-curvature is the range of curvature defined from $FDCF(i)$ as a set of curvatures ranging in $[\kappa_{i,inf}, +\infty[$ for both sides of the line $c_i + tv_i^1$ and 0 on $c_i + tv_i^1$ (see Figure 19). For dyadic points, the pseudo-curvature can be obtained straightforwardly from the self-similarity property and previous results from the endpoints of the curve. For example, to determine the pseudo-curvature at the joining point ($T_0c_1 = T_1c_0$), we just have to apply the operator T_0 on $FDCF(1)$ and T_1 on $FDCF(0)$ to obtain the left and the right pseudo-curvature, which is for the left pseudo-curvature:

$$\kappa_L(t) = \frac{\left\| PT_0 D'_{T_1, q_0}(t) \times PT_0 D''_{T_1, q_0}(t) \right\|}{\left\| PT_0 D'_{T_1, q_0}(t) \right\|^3}. \quad (16)$$

For the right side of the joining point, $\kappa_R(t)$ is deduced from equation 16 by interchanging T_0 and T_1 . It is equivalent to computing the pseudo-curvature of

a new projection according to the control point $P' = PT_1$. For any dyadic point $p = T_{\sigma_0} T_{\sigma_1} \dots T_{\sigma_{l-1}} c_{\sigma_l}$ we have:

$$\kappa_L(t) = \frac{\left\| PTT_0 D'_{T_1, q_0}(t) \times PTT_0 D''_{T_1, q_0}(t) \right\|}{\left\| PTT_0 D'_{T_1, q_0}(t) \right\|^3}, \quad (17)$$

where $T = T_{\sigma_0} T_{\sigma_1} \dots T_{\sigma_{l-2}}$. For the right side of the dyadic point p , $\kappa_R(t)$ is deduced from equation 17 by interchanging T_0 and T_1 . Note that if $\sigma_l = 0$, we have $\sigma_{l-1} = 1$ because of the definition of a dyadic point. Consequently $T_{\sigma_0} T_{\sigma_1} \dots T_{\sigma_{l-2}} T_1 c_0 = T_{\sigma_0} T_{\sigma_1} \dots T_{\sigma_{l-2}} T_0 c_1 = p$. We have the symmetric property if $\sigma_l = 1$.

Figure 17 shows in orange the resulting range of osculating circles representing the right pseudo-curvature at the joining point (see Figure 18 for its left pseudo-curvature). Also, Figure 19 shows the range of osculating circles at the joining point for the case where $\lambda_i^1 < 0$ and $\lambda_i^2 > 0$ (Figure 19).

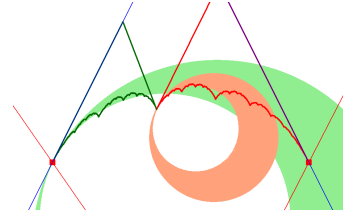


Figure 17: First, $FDCF(0)$ of the curve in Figure 15 induces a range of osculating circles (illustrated in green) at the left endpoint c_0 , where $\kappa_{0,inf} = 1.492$, $\kappa_{0,sup} = 0.982$. Second, the range of osculating circles for the right pseudo-curvature at the joining point is illustrated in orange, where $2.008 \leq \kappa \leq 2.932$. For this curve: $\lambda_0^2 = (\lambda_0^1)^2 = 0.3025$ ($1 > \lambda_0^1 > \lambda_0^2 > 0$).

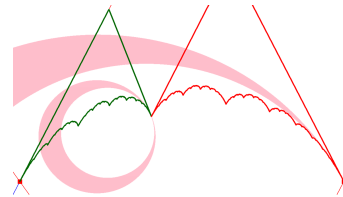


Figure 18: In pink, we show the range of the left pseudo-curvature (of the curve displayed in Figure 15) at c_1 : $0.589 \leq \kappa \leq 0.733$ and at the joining point $= T_0c_1$: $2.785 \leq \kappa \leq 3.460$. For this curve: $\lambda_1^2 = (\lambda_1^1)^2 = 0.49$ ($1 > \lambda_1^1 > \lambda_1^2 > 0$).

Figures 20 to 22 show some examples of fractal curves defined from the same set of control points. For information, we display their associated osculating circles, distribution of normals (on the top right corner in black), and we mention their fractal dimension.

First, we consider the case where $\alpha = 2$. Figures

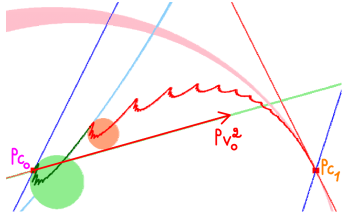


Figure 19: In green, osculating circles representing the range of the right curvatures at the left endpoint c_0 : $5.555 < \kappa < +\infty$, for both sides of $P_{c_0} + tP_{v_0^a}$, and $\kappa = 0$ on $P_{c_0} + tP_{v_0^a}$. In pink, the left range of osculating circles at the right endpoint c_1 ($0.478 \leq \kappa \leq 0.525$). In orange and blue, the right and left ranges of osculating circles at the joining point ($9.492 < \kappa < +\infty$ and $0.115 \leq \kappa \leq 0.126$ respectively). For this curve: $\lambda_0^1 = -0.35$ and $\lambda_0^2 = (\lambda_0^1)^2$.

20 and 21 show two symmetric curves having different right and left tangents at the joining point (red and green lines in the figures), but since each curve is symmetric, i.e. the operators have the same eigenvalues and eigenvectors, then we have equal ranges of the left and right curvatures (κ_L and κ_R).

In the specific case where T_0 and T_1 represent the de Casteljau matrices, we obtain a Bézier curve, with a unique DCF which is the Bernstein polynomial basis functions.

Secondly, when $\alpha > 2$, $\kappa_L = \kappa_R = 0$, meaning the osculating circle is a straight line. Figure 22 left shows a fractal curve for which at, any point, the curve seems to jump suddenly in the direction of the tangent, which corresponds to the osculating “circle” (see the endpoints and the joining point). Finally, when $1 < \alpha < 2$, $\kappa_L = \kappa_R = +\infty$, meaning the osculating circle is reduced to a point. Figure 22 right shows a fractal curve for which, at any point, the curve seems to turn sharply in a different direction from the tangent.

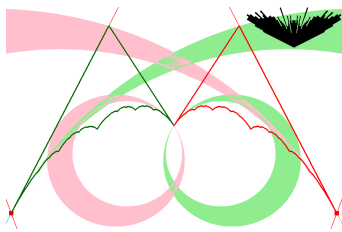


Figure 20: At the joining point, we display the right and left sets of osculating circles with: $2.375 \leq \kappa_R = \kappa_L \leq 2.958$. For this curve: the fractal dimension is 1.021. $\alpha_{i,2} = 2$ and $\lambda_i^2 = (\lambda_i^1)^2 = 0.36$.

From the previous Figures (17 to 22), we can observe a dependency between the amplitude of the pseudo-curvature range and the curve’s apparent roughness, as the values of the fractal dimension show.

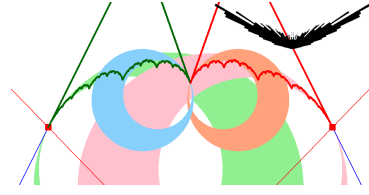


Figure 21: At the joining point, we display the right and left sets of osculating circles with: $2.808 \leq \kappa_R = \kappa_L \leq 4.098$. For this curve: the fractal dimension is 1.095, $\alpha_{i,2} = 2$ and $\lambda_i^2 = (\lambda_i^1)^2 = 0.4225$.

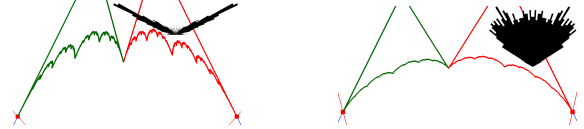


Figure 22: For these two figures, we focus on the joining point. Left: $\alpha_{i,2} = 3 \Rightarrow \kappa_L = \kappa_R = 0$, the fractal dimension is 1.052, $\lambda_i^2 = 0.343$ and $\lambda_i^1 = 0.7$. Right: $1 < \alpha < 1.5 < 2 \Rightarrow \kappa_L = \kappa_R = +\infty$, the fractal dimension is 1.007, $\lambda_0^2 = 0.3536$, $\lambda_0^1 = 0.5$, $\lambda_1^2 = 0.4079$ and $\lambda_1^1 = 0.55$.

7 DISCUSSION

The DCF has two main interests. First, it highlights the dynamical behavior of the IFS; we mean how an operator matches a point of the curve onto another one along the iteration process, up to the limit fixed point. The DCF helps to understand and characterize the differential properties of the curve, as we have shown for the pseudo-tangent and curvature, which significantly impacts the roughness. Second, the DCF is defined from the IFS operators’ eigensystems. Consequently, we can fix the eigenvalues and eigenvectors to obtain desired differential properties. Denoting D the diagonal matrices of expected eigenvalues and V , the column matrix of the chosen independent eigenvectors, we can compute the matrix M of the corresponding operator by $M = VD V^{-1}$. The eigenvalue λ_1 and its associated eigenvector define the tangent at the fixed point. Then, we can choose the value of α by setting $\lambda_2 = \pm \lambda_1^\alpha$ ($\alpha = \frac{\log(|\lambda_2|)}{\log(|\lambda_1|)}$) to specify the type of curvature ($\alpha < 2 \Rightarrow \kappa = \infty$, $\alpha > 2 \Rightarrow \kappa = 0$, $\alpha = 2 \Rightarrow$ range of curvatures).

Specifying tangents and curvatures at endpoints (fixed points) is insufficient to control the roughness accurately. The joining point of the two self-similar curve parts plays a crucial role. Its right and left pseudo-tangents depend continuously on the endpoints pseudo-tangents. By adjusting their relative orientations, we can define a more or less sharp peak (or valley), which will be copied along the curve by self-similarity (see Figure 23 left). In (Podkorytov, 2013), Podkorytov shows how to impose $G^{(1)}$ continuity on curves defined by C-IFS. Using this approach

and choosing appropriate eigenvalues and eigenvectors, we can define different left and right curvatures at the joining point. The resulting curve is $G^{(1)}$ with a specific "second-order" roughness (see Figure 23 right).

In this paper, we give priority to didactic simple examples. However, complex curves and surfaces can be produced by increasing the degrees of freedom (d.o.f) using more than two operators and more control points. The deterministic self-similarity aspect is not visible with just a few more d.o.f, producing random-like curves and surfaces (see Figures 24 and 25 right). Our results remain for any configurations, and we have to proceed to a deep study to understand the relation between pseudo-curvature and roughness.

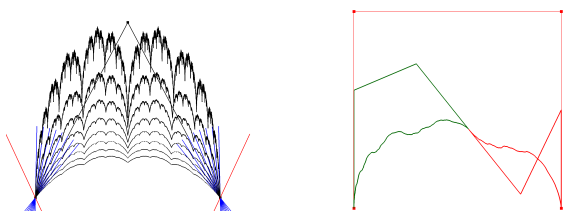


Figure 23: Left: a family of curves sharing their second eigenvectors (in red) with different orientations of the pseudo-tangents at endpoints (in blue). The variation of the valley sharpness, induced by the pseudo-tangent variation, impacts the roughness. Right: a $G^{(1)}$ continuity curve with a "second-order" roughness.

8 CONCLUSION

In this study, we propose a method to address the second derivative behavior of fractal curves by introducing a notion of pseudo-curvature. By fractal curves, we mean self-similar curves described with iterated function systems (IFS). These curves are completely defined from the set of operators of the IFS and result from a deterministic iterative process. We introduce the *differential characteristic function (DCF)* as a central tool to analyze the differential behavior of the iterative computations. We define a family of *DCFs* which abstracts the complexity of the iterative process around each fixed point. Finally, from this family of *DCFs*, we obtain a range of curvatures defining the pseudo-curvature of the fractal curve. We study the different configurations of possible pseudo-curvatures according to operators' eigenvalues and eigenvectors. These results, stated for fixed points, are propagated to dyadic points thanks to the self-similarity property. We provide examples of various differential situations of fractal curves. The illustrations show, quali-

tatively, the relevance of this pseudo-curvature, as the range of osculating circles closely matches the curve. Note that all results are illustrated with planar fractal curves, but computations are conducted without such an assumption. All results remain valid for a non coplanar set of control points defined in \mathbb{R}^3 , inducing a non planar curve. Independently of the differential property, the *DCF* is a useful tool to leverage geometric intuition to facilitate the analysis of self-similar fractals.

These results should be straightforwardly extended to tensor product surfaces. Their bidirectional structuration generally induces combinations of unidirectional configurations. However, we must focus carefully on non-tensor surfaces, which are more complex constructions that generate surfaces with random appearances (see Figure 25). For example, complex eigenvalues avoided for curves will produce interesting vortex effects for surfaces.

We also have to study the relation between the roughness and the differentiable characteristics in detail. Roughness is characterized by oscillation frequency (depending on the operator contraction) and oscillation amplitude (depending on the pseudo-tangent and curvature range). We need to formalize these relations to provide an intuitive and accurate control of roughness.

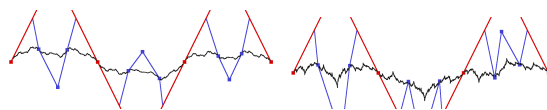


Figure 24: Example of two curves designed with 3 operators and 7 control points.

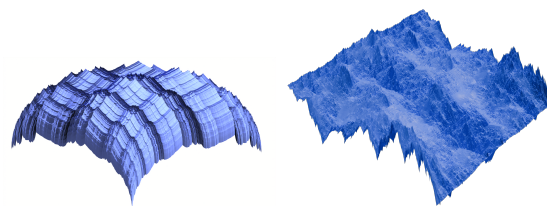


Figure 25: Left: tensor product surface created from a fractal curve. Right: a more complex non-tensor product fractal surface, built from 4 operators and 8 control points.

9 ACKNOWLEDGEMENTS

This work benefited from the support of the project Fraclettes ANR-20-CE46-0003 of the French National Research Agency (ANR).

REFERENCES

- Allaart, P. C. and Kawamura, K. (2010). The improper infinite derivatives of takagi's nowhere-differentiable function. *Journal of Mathematical Analysis and Applications*, 372(2):656–665.
- Allaart, P. C. and Kawamura, K. (2012). The takagi function: a survey. *Real Analysis Exchange*, 37(1):1–54.
- Barnsley, M. F. (2014). *Fractals everywhere*. Academic press.
- Bensoudane, H. (2009). *Etude différentielle des formes fractales*. PhD thesis, Université de Bourgogne.
- Bensoudane, H., Gentil, C., and Neveu, M. (2009). Fractional half-tangent of a curve described by iterated function systems. *Journal Of Applied Functional Analysis*, 4(2):311–326.
- Bigerelle, M., Nianga, J.-M., Najjar, D., Iost, A., Hubert, C., and Kubiak, K. (2013). Roughness signature of tribological contact calculated by a new method of peaks curvature radius estimation on fractal surfaces. *Tribology International*, 65:235–247.
- Bolzano, B. (1851). *Paradoxes of the Infinite*. Leipzig, C.H. Reclam.
- Cavalier, A., Gilet, G., and Ghazanfarpour, D. (2019). Local spot noise for procedural surface details synthesis. *Computers and Graphics*, 85:92–99.
- Chermain, X., Sauvage, B., Dischler, J.-M., and Dachsbacher, C. (2021). Importance sampling of glittering BSDFs based on finite mixture distributions. In *Proc. of Eurographics Symposium on Rendering*, pages 45–53.
- Cook, R. L. and DeRose, T. (2005). Wavelet noise. *ACM Trans. Graph.*, 24(3):803–811.
- Daoudi, K., Lévy Véhel, J., and Meyer, Y. (1998). Construction of continuous functions with prescribed local regularity. *Constructive Approximation*, 14:349–385.
- Fournier, A., Fussell, D., and Carpenter, L. (1982). Computer rendering of stochastic models. *Communications of the ACM*, 25(6):371–384.
- Gentil, C., Gouaty, G., and Sokolov, D. (2021). *Geometric Modeling of Fractal Forms for CAD*. John Wiley & Sons.
- Gilet, G., Sauvage, B., Vanhoey, K., Dischler, J.-M., and Ghazanfarpour, D. (2014). Local random-phase noise for procedural texturing. *ACM Trans. Graph.*, 33(6):1–11.
- Hardy, G. H. (1916). Weierstrass's non-differentiable function. *Transactions of the American Mathematical Society*, 17(3):301–325.
- Hu, Y. Z. and Tonder, K. (1992). Simulation of 3-D random rough surface by 2-D digital filter and fourier analysis. *International Journal of Machine Tools and Manufacture*, 32(1-2):83–90.
- Hutchinson, J. (1981). Fractals and self-similarity. *Indiana Univ. Math. J.*, 30:713–747.
- Lagae, A., Lefebvre, S., Drettakis, G., and Dutré, P. (2009). Procedural Noise using Sparse Gabor Convolution. *ACM Transactions on Graphics*, 28(3):54–64.
- Mandelbrot, B. B. (1977). *Fractals: Form, Chance, and Dimension*. W.H. Freeman.
- Moalic, H., Fitzpatrick, J., and Torrance, A. (1987). The correlation of the characteristics of rough surfaces with their friction coefficients. *Proc. of the Institution of Mechanical Engineers, Part C: Journal of Mechanical Engineering Science*, 201(5):321–329.
- Morlet, L., Gentil, C., Lanquetin, S., Neveu, M., and Baril, J.-L. (2019). Representation of nurbs surfaces by controlled iterated functions system automata. *Computers & Graphics*, 2:100006.
- Nayak, S. R., Mishra, J., and Palai, G. (2019). Analysing roughness of surface through fractal dimension: A review. *Image Vis. Comput.*, 89:21–34.
- Nowicki, B. (1985). Multiparameter representation of surface roughness. *Wear*, 102(3):161–176.
- Pavie, N. (2016). *Modélisation par bruit procédural et rendu de détails volumiques de surfaces dans les scènes virtuelles*. PhD thesis, Université de Limoges.
- Perlin, K. (1985). An image synthesizer. *SIGGRAPH Comput. Graph.*, 19(3):287–296.
- Podkorytov, S. (2013). *Tangent spaces for self-similar shapes*. Phd thesis, Université de Bourgogne.
- Pérez-Ráfols, F. and Almqvist, A. (2019). Generating randomly rough surfaces with given height probability distribution and power spectrum. *Tribology International*, 131:591–604.
- Schaefer, S., Levin, D., and Goldman, R. (2005). Subdivision Schemes and Attractors. *Symposium on Geometry Processing*, pages 171–180.
- Sokolov, D., Gouaty, G., Gentil, C., and Mishkinis, A. (2015). Boundary controlled iterated function systems. In *Curves and Surfaces: 8th International Conference, Paris*, pages 414–432.
- Stam, J. (2001). An illumination model for a skin layer bounded by rough surfaces. In *Proc. of the Eurographics Workshop on Rendering Techniques*, page 39–52.
- Thim, J. (2003). *Continuous Nowhere Differentiable Functions*. Master's thesis, Luleå University of Technology.
- Walter, B., Marschner, S. R., Li, H., and Torrance, K. E. (2007). Microfacet models for refraction through rough surfaces. In *Proc. of the Eurographics Conference on Rendering Techniques*, page 195–206.
- Wang, Y., Azam, A., Wilson, M. C., Neville, A., and Morina, A. (2021). Generating fractal rough surfaces with the spectral representation method. *Proc. of the Institution of Mechanical Engineers, Part J: Journal of Engineering Tribology*, 235(12):2640–2653.
- Warszawski, K. K., Nikiel, S. S., and Mrugalski, M. (2019). Procedural method for fast table mountains modelling in virtual environments. *Applied Sciences*, 9(11).
- Whitehouse, D. J. (1982). In *Rough surfaces (Ed. T. R. Thomas)*. Digital techniques.
- Zair, C. E. and Tosan, E. (1996). Fractal modeling using free form techniques. *Computer Graphics Forum*, 15(3):269–278.